Editors' Suggestion

Unified Model for Size-Dependent to Size-Independent Transition in Yield Strength of Crystalline Metallic Materials

Wenbin Liu,[1] Ying Liu,[1] Yangyang Cheng,[1] Lirong Chen,[1] Long Yu,[1] Xin Yi,[1] and Huiling Duan[1,2,*]
[1]State Key Laboratory for Turbulence and Complex Systems, Department of Mechanics and Engineering Science, BIC-ESAT, College of Engineering, Peking University, Beijing 100871, People's Republic of China
[2]CAPT, HEDPS, and IFSA Collaborative Innovation Center of MoE, Peking University, Beijing 100871, People's Republic of China

(Received 4 January 2020; revised manuscript received 14 May 2020; accepted 18 May 2020; published 9 June 2020)

Size-dependent yield strength is a common feature observed in miniaturized crystalline metallic samples, and plenty of studies have been conducted in experiments and numerical simulations to explore the underlying mechanism. However, the transition in yield strength from bulklike to size-affected behavior has received less attention. Here a unified theoretical model is proposed to probe the yield strength of crystalline metallic materials with sample size from nanoscale to macroscale. We show that the transition in yield strength versus size can be fully explained by the competition between the stresses required for dislocation source activation and dislocation motion, which is regulated by dislocation density, irradiation defect, grain boundary, and so on. Based on various grain boundary densities, the extended Hall–Petch relation, incorporated into the unified model, captures the reverse size effect for polycrystalline samples. The proposed model predictions agree well with reported experimental measurements of various specimens, including the prestrained nickel, irradiated copper, ultrafine grain tungsten, and so on.

DOI: 10.1103/PhysRevLett.124.235501

Understanding mechanical properties of crystalline metallic materials at the small length scale is important for designing and fabricating mechanically reliable nanodevices and nanostructures [1]. Size-dependent yielding, as a well-known phenomenon, is widely observed in the uniaxial tension or compression tests on micropillars [2–8]. Compared with bulk samples, higher stress is required in miniaturized samples during plastic deformation [5–7,9–13]. In the past few decades, abundant studies demonstrated that the yield strength obeys a power law relation with respect to the specimen size in microscale regime and can be understood in terms of the dislocation source-limited mechanism [12–18]. Namely, the dislocation generation becomes harder at the small length scale [16,17], and escape of dislocations near the free surfaces causes the dislocation starvation or exhaustion, so a higher stress is needed to activate new dislocation sources [4,18–20]. The critical resolved shear stress (CRSS) τ_c of miniaturized materials, characterizing the yield strength σ_y, is generally adopted as the following simple linear form in most existing models [15,17,21–24]:

$$\tau_c = \tau_m + \tau_s. \tag{1}$$

Here τ_m denotes the stress required for dislocation motion, which is usually regarded as the bulk CRSS, and τ_s represents the contribution of dislocation source hardening. For crystalline materials, τ_s can be described by a power law $\tau_s = K\mu b d^{-m}$ [15], where μ is the material shear modulus, b is the magnitude of Burgers vector, d is the grain size, K and m are the material parameters associated with stacking fault energy [6,25], temperature [7,15], dislocation source density [19], and so on. Although the size dependence of yield strength or CRSS at nanoscale or microscale has been captured by Eq. (1) [15,17,22,23], the transition from a size-dependent to size-independent yield strength is veiled [18,26], especially in prestrained nickel (Ni) [27], irradiated copper (Cu) [9], high strength Ni alloy [28], and tungsten (W) [11].

Besides the size-dependent yield strength depicted by the thick (red) line in Fig. 1, in the microtesting of one-dimensional polycrystalline materials such as nanowires and micropillars, the reverse size effect that the yield strength increases with increasing sample diameter has

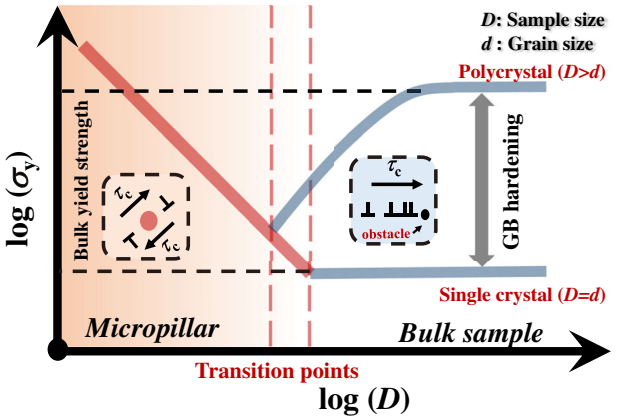

FIG. 1. Schematic of yield strength σ_y as a function of the sample size D.

 © 2020 American Physical Society

been reported [11,29,30] as indicated by the thin (gray) line in Fig. 1.

In this work, we propose a unified model to probe the yield strength of crystalline metallic materials in a wide sample size range at a fundamental level. For single crystals, a novel yielding mechanism is presented that the yield strength depends on the competition between stresses required for dislocation motion and dislocation source activation. This competition model is fundamentally different from the model in previous works where the source activation stress is considered as a part of superposition form. Moreover, we extend the classical Hall–Petch relation to the microsize polycrystals based on the evolution of grain boundary (GB) density. We then propose a model to describe the yield strength of single crystals and polycrystals analytically.

It is well known that the hardening effects of bulk materials arise from different aspects of material microstructures. For example, the lattice friction, dislocation forest, GB, and irradiation defect are generally regarded as the obstacles for dislocation motion, and they together contribute to the stress τ_m required for dislocation motion following the superposition principle [23,31]. Different from the bulk materials, the size effect of miniaturized samples is controlled by dislocation source-limited mechanism. At the small length scale, the limited dislocation source activation leads to a lack of mobile dislocations, which further causes the increasing yield strength, i.e., source hardening effect τ_s. At $\tau_s \gg \tau_m$, the yielding model in superposition form [Eq. (1)] is valid to model the size-dependent yield strength [15,17,21–23]. However, in the cases where τ_s and τ_m are at the same order, Eq. (1) has difficulty in explaining the experimental results [9,11,27,28], which are depicted as the transition behaviors in Fig. 1.

Focusing on physical mechanisms of size-dependent yield strength of crystalline metallic materials, here we hypothesize that the yield strength of material characterized by the CRSS τ_c is dominated by the competition between the activation of dislocation source and motion of dislocations as given in Eq. (2)

$$\tau_c = \max(\tau_m, \tau_s) = \max(\tau_f + \tau_{\mathrm{dis}}, \tau_s) \tag{2}$$

with τ_m depending on the lattice friction stress τ_f and dislocation forest hardening stress τ_{dis}. Here τ_{dis} can be represented as $\tau_{\mathrm{dis}} = \alpha\mu b\sqrt{\rho_{\mathrm{dis}}}$, where ρ_{dis} denotes the dislocation density and α is the material constant. Equation (2) points out that the plastic deforming in crystalline metallic materials needs to satisfy the following requirements. First, the stress on dislocations is sufficient to overcome the obstacles on the slip plane, and second, dislocation source could continuously emit dislocation. For pure single crystals, Eq. (2) can be rewritten as

$$\tau_c = \max(\tau_f + \alpha\mu b\sqrt{\rho_{\mathrm{dis}}}, K\mu b d^{-m}), \tag{3}$$

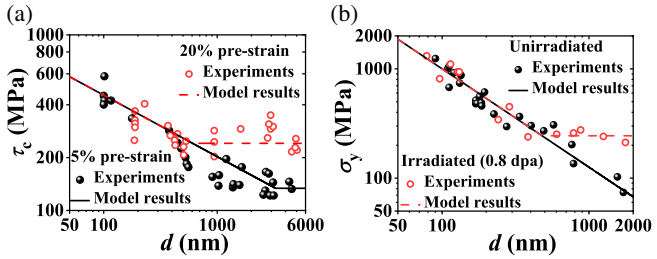

FIG. 2. CRSS τ_c/Yield strength σ_y as a function of pillar diameter for (a) Ni single crystal at different prestrains and (b) irradiated and unirradiated Cu single crystals. Symbols represent experimental data from Refs. [9] and [27].

where $\tau_m = \tau_f + \alpha\mu b\sqrt{\rho_{\mathrm{dis}}}$ is adopted to be independent of the sample size [15,17]. Note that the proposed model is not applicable for the dislocation-free whisker owing to the absence of dislocation source [6,12,15].

Equation (3) is verified by microcompression tests on micropillars of prestrained Ni single crystal [27]. The size-dependent CRSS of Ni micropillars of different diameters d has been measured at prestrains of 5% and 20%. A larger prestrain corresponds to a higher dislocation density [27]. In Fig. 2(a), we compare measured τ_c of nickel micropillars of different diameters d at 5% and 20% prestrains with our theoretical prediction (model parameters listed in Table I). Here we ignore the lattice friction stress τ_f of face-centered cubic materials at room temperature [23]. It is shown that Eq. (3) with $\rho_{\mathrm{dis}} = 2 \times 10^{14}$ m^{-2} and 6.5×10^{14} m^{-2} adopted at 5% and 20% prestrains, respectively, agrees well with experimental results with measured ρ_{dis} of 3.7×10^{14} m^{-2} and 4.5×10^{14} m^{-2} [27]. The CRSS of both samples exhibits significant size effect at relatively small sizes. As the sample size d exceeds certain values (around 500 nm and 3000 nm at 5% and 20% prestrains, respectively), CRSS becomes size independent because τ_s is less than τ_m. The length scale of the transition of CRSS from size dependent to size independent decreases as the dislocation density increases, which is consistent with the dislocation dynamics simulations [26].

The transition in yield strength from size dependent to size independent can also be observed in the microcompression tests of irradiated single crystal Cu [9]. As shown in Fig. 2(b), the irradiated Cu micropillars present a transition behavior at submicroscale (around 500 nm), whereas the unirradiated ones of the same size still display size effect. In previous studies, the resistance of irradiation defects to dislocation motion has been described by $\beta\sqrt{N_{\mathrm{def}} d_{\mathrm{def}}}$, where β is the hardening coefficient, and N_{def} and d_{def} are, respectively, the average density and size of the irradiation defect [23,33,34]. Therefore, the CRSS τ_c^{irr} of the irradiated single crystals is proposed as

$$\tau_c^{\mathrm{irr}} = \max(\tau_f + \alpha\mu b\sqrt{\rho_{\mathrm{dis}}} + \beta\sqrt{N_{\mathrm{def}} d_{\mathrm{def}}}, K\mu b d^{-m}). \tag{4}$$

TABLE I. Parameters for model prediction of Ni and Cu single crystals.

Materials	μ(GPa)	b(nm)	$K(\mathrm{m}^{m-1})$	m	α	β(N/m)	$N_{\mathrm{def}}(10^{23}\ \mathrm{m}^{-3})$	d_{def}(nm)
Ni	76[a]	0.249[a]	8.5×10^4	0.35	0.5[a]	…	…	…
Cu	48.3[a]	0.255[a]	17	0.9	0.5[a]	0.224	4.5[b]	2.5[b]

Parameters with superscripts a and b are adopted from Refs. [32] and [23], respectively.

The dislocation density ρ_{dis} here is adopted as $2\times10^{12}\ \mathrm{m}^{-2}$ [23]. Because the yield stress is measured under the loading direction [100] in experiments, we have $\sigma_y^{\mathrm{irr}}=\tau_c^{\mathrm{irr}}/R$ with $R=0.408$ as the corresponding Schmid factor. Figure 2(b) shows that Eq. (4) agrees well with experimental results (model parameters listed in Table I). In addition to the transition behavior of yield strength in both irradiated and unirradiated Cu, the absence of irradiation hardening effect in irradiated Cu at $d<500$ nm validates Eq. (4). At $\tau_s>\tau_m$, the yield strength is dominated by τ_s, so unirradiated and irradiated samples could exhibit the same yield strength.

From the case studied above, one can see that the transition point (Fig. 1) in miniaturized single crystals decreases as the stress required for dislocation motion increases. Besides the prestrained Ni and irradiated Cu single crystals, Eq. (2) is also valid for high strength Ni-based alloy, in which a high constant yield strength is observed for diameters ranging from 200 nm to 4 μm [28] (see Fig. S1 in Supplemental Material [35]). This model enriches our understanding of the appearance or disappearance of the size effect for Ni-based alloy micropillars [28,36–38].

Once the sample size exceeds the transition point (Fig. 1), the miniaturized polycrystalline materials ($d<D$) generally display a reverse size effect such that yield strength decreases with a decreasing sample size [29,30]. To explain the reverse size effect, Yang *et al.* [29] suggested that the yield strength of the region near the free surface is smaller than that of the interior region and proposed a mixture model to characterize the yield strength of miniaturized polycrystalline copper wires, which agreed well with experiments [30]. However, there exist several artificial fitting parameters in the model that further inspire one to consider whether there is a better theoretical model.

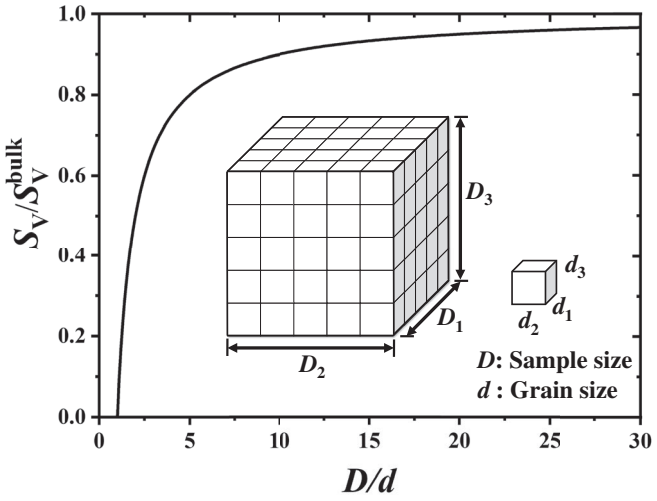

FIG. 3. Normalized GB density S_V/S_V^{bulk} as a function of D/d. Embedded graph shows a simplified illustration of polycrystalline materials.

In this study, the reverse size effect is attributed to the increases of the proportion of GBs, which could increase the yield strength by hindering dislocation motion. For bulk polycrystalline materials, the classical Hall–Petch relation [39,40] is widely applied to describe the GB hardening effect. Here we propose an analytical model based on the Hall–Petch relation to investigate the size-dependent yield strength of miniaturized polycrystalline materials. The classical Hall–Petch relation has the general form [39,40]

$$\tau_c=\tau_0+k\sqrt{\frac{1}{d}}, \tag{5}$$

where k is material constant, d is the characteristic grain size, and $\tau_0=\tau_f+\tau_{\mathrm{dis}}$ is a combination of intrinsic lattice resistance and dislocation hardening stress for pure metallic materials. It is noted that $1/d$ is proportional to GB density (GB area per unit volume) [32]. Thus, Eq. (5) can be rewritten as [31,41]

$$\tau_c=\tau_0+k^*\sqrt{S_V}, \tag{6}$$

where $S_V\propto 1/d$ is defined as GB density. Note that the value of GB density in miniaturized samples is also associated with sample size. The inset in Fig. 3 provides a schematic illustration of the polycrystalline materials in which the geometric shape of each grain is set to be a cube. Then, the corresponding GB density can be determined by

$$S_V=\sum_{n=1}^{3}\left(\frac{1}{d_n}-\frac{1}{D_n}\right). \tag{7}$$

Using the harmonic mean of grain sizes $3/\sum_{n=1}^{3}1/d_n$ and harmonic mean of sample sizes $3/\sum_{n=1}^{3}1/D_n$ to effectively represent the grain size d and sample size D, Eq. (7) can be written as $S_V=3(1/d-1/D)$. To cover the variety of grain shapes, we introduce a grain shape coefficient ξ and rewrite Eq. (7) as

$$S_V=\xi\left(\frac{1}{d}-\frac{1}{D}\right) \tag{8}$$

with $\xi \approx 2$ for columnar grains and $\xi \approx 3$ for equiaxed grains. The normalized GB density can then be expressed as $S_V/S_V^{\text{bulk}} = 1 - d/D$ with $S_V^{\text{bulk}} = \xi/d$. Figure 3 shows S_V/S_V^{bulk} as a function of D/d. The GB density increases rapidly at $D/d < 5$ and gradually saturates at $D/d > 15$.

Substituting Eq. (8) into Eq. (6), we have

$$\tau_c = \tau_0 + k\sqrt{\frac{1}{d} - \frac{1}{D}}. \tag{9}$$

Here the material parameter $k(=\xi k^*)$ is associated with the grain shape and material properties. The modified Hall–Petch relation includes not only the grain size d but also the sample size D. At $d = D$, Eq. (9) reduces to $\tau_c = \tau_0$ without GB effect. At $d \ll D$, Eq. (9) reduces to the classical Hall–Petch relation in Eq. (5).

Note that only the homogeneous materials are discussed here. For the gradient-structured polycrystals, GB density is a function of spatial location [42]. Similar to the classical Hall–Petch relation, a restriction of Eq. (9) is that it cannot be applied to samples with grain size on the order of 10 nm whose plastic deformation is mediated by GB motions such as GB migration, GB sliding, and grain rotation [43–45].

Equation (9) is verified with experiments on Cu [29,46,47] and austenitic stainless steel [5,30] polycrystals. To normalize the experimental data for different materials [29,30], we analyze the size effect using the normalized yield strength $\sigma_y/\sigma_y^{\text{bulk}}$ as

$$\frac{\sigma_y}{\sigma_y^{\text{bulk}}} = \frac{M\left(\tau_0 + k\sqrt{\frac{1}{d} - \frac{1}{D}}\right)}{M\left(\tau_0 + k\sqrt{\frac{1}{d}}\right)} = \frac{\tau_0 + k\sqrt{\frac{1}{d} - \frac{1}{D}}}{\tau_0 + k\sqrt{\frac{1}{d}}}. \tag{10}$$

Here σ_y^{bulk} denotes the bulk yield strength, and M is the Taylor factor for the cubic polycrystalline materials [48]. For polycrystal materials including limited number of grains, the Taylor factor depends on not only the grain orientations but also the loading direction and is not a constant. As it is quite difficult to determine the value of M for miniaturized samples, here $M \approx 3$ is taken as in most of the literature [48] to simplify the calculation.

$\sigma_y/\sigma_y^{\text{bulk}}$ is plotted in Fig. 4 as a function of D/d for Cu ($d = 3$ μm and $\tau_0 = 10$ MPa) and austenitic stainless steel ($d = 0.6$ μm and $\tau_0 = 200$ MPa) polycrystal samples. In the experiments, the grain size of Cu polycrystals is from 3 μm to 150 μm [29,46,47]; the grain size of austenitic stainless steels [5,30] falls in a range from 0.6 μm to 90 μm. As τ_0 depends on the initial dislocation densities, here to explore the role of the microstructure in evolution of $\sigma_y/\sigma_y^{\text{bulk}}$, different values of d and τ_0 are adopted in our model predictions (see Fig. S2 in Supplemental Material [35]). It is shown that, for both Cu and austenitic stainless steels, the reverse size effect becomes slightly less obvious as d and τ_0 increase, which is attributed to the reduction in the contribution of GB hardening in yield strength.

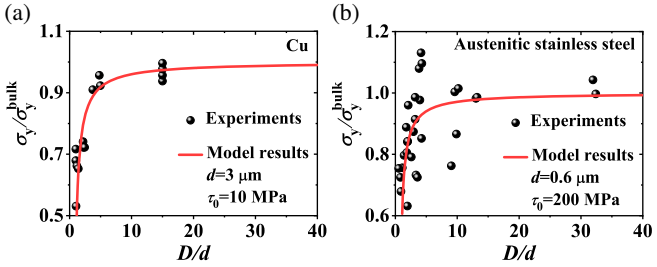

FIG. 4. Size dependence of normalized yield stress $\sigma_y/\sigma_y^{\text{bulk}}$ for (a) Cu [29] and (b) austenitic stainless steel [30] polycrystal samples. The material constant k is taken as 0.06 MPa $\cdot \sqrt{\text{m}}$ and 0.2 MPa $\cdot \sqrt{\text{m}}$ for Cu and austenitic stainless steel, respectively.

Our analytical predictions given by Eq. (10) agree well with experimental results, indicating that the proposed model could effectively describe the size dependence of yield strength for polycrystalline samples. At $D/d < 5$, $\sigma_y/\sigma_y^{\text{bulk}}$ increases rapidly with increasing D/d and the reverse size effect is strong, consistent with the trend in Fig. 3. The yield strength increases with GB density. At $D/d > 15$, $\sigma_y/\sigma_y^{\text{bulk}}$ is close to 1 as expected, attributed to the saturation of GB density.

GB hardening effect arises from the resistance of GB to dislocation motion. Substituting Eqs. (3) and (9) into Eq. (2), a modified yield model can then be given as

$$\tau_c = \max\left(\tau_f + \alpha\mu b\sqrt{\rho_{\text{dis}}} + k\sqrt{\frac{1}{d} - \frac{1}{D}}, K\mu b d^{-m}\right). \tag{11}$$

Eq. (11) is more general and could describe the yield strength for single crystal and polycrystalline materials with sample size ranging from nano-length to macro-length scale.

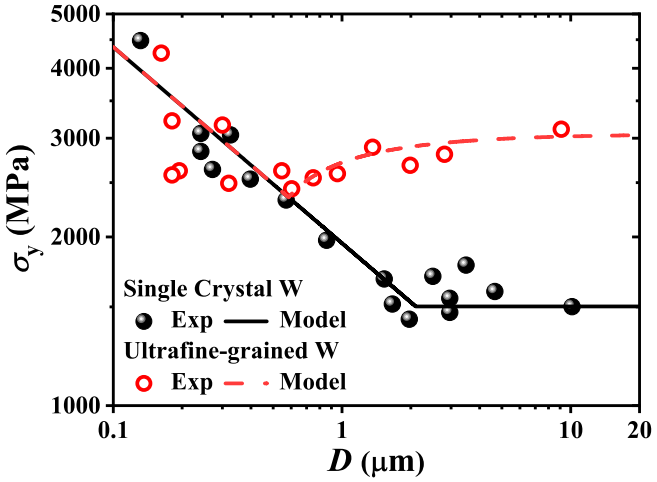

FIG. 5. Size-dependent yield stresses σ_y for the single crystal and ultrafine grain W. Symbols represent experimental data from Ref. [11].

TABLE II. Parameters for model prediction of W.

Materials	τ_f(MPa)	μ(GPa)	b(nm)	$K(\mathrm{m}^{m-1})$	m	$k(\mathrm{MPa}\sqrt{\mathrm{m}})$	α	$\rho_{\mathrm{dis}}(10^{14}\ \mathrm{m}^{-2})$
Single crystal W	370[a]	153.7[a]	0.274[a]	1.5×10^5	0.35	…	0.45[b]	1.65[c]
Ultrafine grain W	370[a]	153.7[a]	0.274[a]	1.2×10^5	0.35	0.28	0.45[b]	1.65[c]

Parameters with superscripts a, b and c are adopted from Refs. [15], [32], and [11], respectively.

The microcompression tests on single crystal and ultrafine grain W with grain size $d \approx 480$ nm are used to verify Eq. (11) [11]. Figure 5 displays σ_y as a function of D for single crystal and ultrafine grain W, and the experimental results show the same trend as illustrated in Fig. 1. The parameters used are listed in Table II. The Schmid factor is taken as $R = 0.408$ [11] and the Taylor factor is $M \approx 3$ for single crystal W and ultrafine grain W, respectively.

It is shown that Eq. (11) can accurately capture the experimental results and both samples exhibit the transition feature. The yield mechanism of various sample sizes is illustrated in Fig. 1. For single crystals, the transition point of yield strength from size dependent to size independent is at $D \approx 2$ μm, consistent with our prediction. At $D \geq 2$ μm, dislocation motion dominates the yield of materials. For the ultrafine grain W, the yield strength exhibits the size effect that σ_y decreases with D increasing at $D < 500$ nm, and the sample size is smaller than the initial grain size 480 nm. Therefore, it can be regarded as a single crystal, and its yield strength is the same as that of single crystals. As D exceeds 500 nm, the yield stress of ultrafine grain W displays the reverse size effect, indicating the increases of GB density. On the other hand, it also demonstrates the transition of the yield strength of ultrafine grain W from dislocation source controlled to dislocation motion controlled.

Equation (11) also suggests that the polycrystalline samples will not display the GB hardening effect at $\tau_m \leq \tau_s$. Such predictions have been observed in the Cu bi-crystal [49–51] and ultrafine grain Cu [52] (as detailed in Figs. S3 and S4 of Supplemental Material [35]).

In summary, we establish a unified model to characterize the yield strength for crystalline metallic materials with sample size from microscales to macroscales. Compared with existing models, the yielding of miniaturized metallic samples in this study needs to satisfy both dislocation motion and dislocation source activation. CRSS can then be determined by the competition between the stresses required for these two mechanisms, so that the transition of yield strength from size dependent to size independent can be captured. As the sample size becomes smaller than the length scale of transition, the yield strength is governed by dislocation source activation stress to exhibit the size dependence. After the source activation stress less than dislocation motion stress, single crystals display the size-independent yield strength, and polycrystals could show the reverse size effect of yield strength owing to increase in GB density. All of these experimental results are accurately captured by the theoretical model. It is revealed that the transition of yield strength from size dependent to size independent is sensitive to microstructures, depending on the contribution of dislocation density, GB density, irradiation defect, dispersoids, and other microstructures to dislocation motion resistance.

The authors thank the National Natural Science Foundation of China (Grants No. 11632001, No. 11521202, No. 11988102, and No. U1830121), the National Science and Technology Major Project (Grant No. 2017-VI-0003-0073), and the Science Challenge Project (Grant No. TZ2018001) for their support.

*Corresponding author.
hlduan@pku.edu.cn

[1] W. D. Nix, J. R. Greer, G. Feng, and E. T. Lilleodden, Deformation at the nanometer and micrometer length scales: Effects of strain gradients and dislocation starvation, Thin Solid Films **515**, 3152 (2007).
[2] M. D. Uchic, D. M. Dimiduk, J. N. Florando, and W. D. Nix, Sample dimensions influence strength and crystal plasticity, Science **305**, 986 (2004).
[3] P. Hosemann, Small-scale mechanical testing on nuclear materials: Bridging the experimental length-scale gap, Scr. Mater. **143**, 161 (2018).
[4] J. R. Greer, W. C. Oliver, and W. D. Nix, Size dependence of mechanical properties of gold at the micron scale in the absence of strain gradients, Acta Mater. **53**, 1821 (2005).
[5] J. R. Greer and J. Th. M. De Hosson, Plasticity in small-sized metallic systems: Intrinsic versus extrinsic size effect, Prog. Mater. Sci. **56**, 654 (2011).
[6] O. Kraft, P. A. Gruber, R. Mönig, and D. Weygand, Plasticity in confined dimensions, Annu. Rev. Mater. Res. **40**, 293 (2010).
[7] A. S. Schneider, D. Kaufmann, B. G. Clark, C. P. Frick, P. A. Gruber, R. Mönig, O. Kraft, and E. Arzt, Correlation Between Critical Temperature and Strength of Small-Scale bcc Pillars, Phys. Rev. Lett. **103**, 105501 (2009).
[8] C. P. Frick, B. G. Clark, S. Orso, A. S. Schneider, and E. Arzt, Size effect on strength and strain hardening of small-scale [111] nickel compression pillars, Mater. Sci. Eng. A **489**, 319 (2008).
[9] D. Kiener, P. Hosemann, S. A. Maloy, and A. M. Minor, In situ nanocompression testing of irradiated copper, Nat. Mater. **10**, 608 (2011).
[10] N.-Y. Park, H.-S. Nam, P.-R. Cha, and S.-C. Lee, Size-dependent transition of the deformation behavior of Au nanowires, Nano Res. **8**, 941 (2015).
[11] D. Kiener, R. Fritz, M. Alfreider, A. Leitner, R. Pippan, and V. Maier-Kiener, Rate limiting deformation mechanisms of

bcc metals in confined volumes, Acta Mater. **166**, 687 (2019).
[12] A. T. Jennings, M. J. Burek, and J. R. Greer, Microstructure Versus Size: Mechanical Properties of Electroplated Single Crystalline Cu Nanopillars, Phys. Rev. Lett. **104**, 135503 (2010).
[13] B. Kondori, A. Needleman, and A. A. Benzerga, Discrete dislocation simulations of compression of tapered micropillars, J. Mech. Phys. Solids **101**, 223 (2017).
[14] Z. W. Shan, R. K. Mishra, S. A. S. Asif, O. L. Warren, and A. M. Minor, Mechanical annealing and source-limited deformation in submicrometre-diameter Ni crystals, Nat. Mater. **7**, 115 (2008).
[15] S.-W. Lee and W. D. Nix, Size dependence of the yield strength of fcc and bcc metallic micropillars with diameters of a few micrometers, Philos. Mag. **92**, 1238 (2012).
[16] S. I. Rao, D. M. Dimiduk, M. Tang, M. D. Uchic, T. A. Parthasarathy, and C. Woodward, Estimating the strength of single-ended dislocation sources in micron-sized single crystals, Philos. Mag. **87**, 4777 (2007).
[17] T. A. Parthasarathy, S. I. Rao, D. M. Dimiduk, M. D. Uchic, and D. R. Trinkle, Contribution to size effect of yield strength from the stochastics of dislocation source lengths in finite samples, Scr. Mater. **56**, 313 (2007).
[18] M. D. Uchic, P. A. Shade, and D. M. Dimiduk, Plasticity of micrometer-scale single crystals in compression, Annu. Rev. Mater. Res. **39**, 361 (2009).
[19] S. I. Rao, D. M. Dimiduk, T. A. Parthasarathy, M. D. Uchic, M. Tang, and C. Woodward, Athermal mechanisms of size-dependent crystal flow gleaned from three-dimensional discrete dislocation simulations, Acta Mater. **56**, 3245 (2008).
[20] D. M. Dimiduk, M. D. Uchic, and T. A. Parthasarathy, Size-affected single-slip behavior of pure nickel microcrystals, Acta Mater. **53**, 4065 (2005).
[21] J. Zhang, K. Kishida, and H. Inui, Specimen size and shape dependent yield strength in micropillar compression deformation of Mo single crystals, Int. J. Plast. **92**, 45 (2017).
[22] Y. Zou, H. Ma, and R. Spolenak, Ultrastrong ductile and stable high-entropy alloys at small scales, Nat. Commun. **6**, 7748 (2015).
[23] X. Xiao, D. Song, J. Xue, H. Chu, and H. Duan, A size-dependent tensorial plasticity model for FCC single crystal with irradiation, Int. J. Plast. **65**, 152 (2015).
[24] S. Korte and W. J. Clegg, Discussion of the dependence of the effect of size on the yield stress in hard materials studied by microcompression of MgO, Philos. Mag. **91**, 1150 (2011).
[25] J. H. Wu, W. Y. Tsai, J. C. Huang, C. H. Hsieh, and G.-R. Huang, Sample size and orientation effects of single crystal aluminum, Mater. Sci. Eng. A **662**, 296 (2016).
[26] J. A. El-Awady, Unravelling the physics of size-dependent dislocation-mediated plasticity, Nat. Commun. **6**, 5926 (2015).
[27] A. S. Schneider, D. Kiener, C. M. Yakacki, H. J. Maier, P. A. Gruber, N. Tamura, M. Kunz, A. M. Minor, and C. P. Frick, Influence of bulk pre-straining on the size effect in nickel compression pillars, Mater. Sci. Eng. A **559**, 147 (2013).
[28] B. Girault, A. S. Schneider, C. P. Frick, and E. Arzt, Strength effects in micropillars of a dispersion strengthened superalloy, Adv. Eng. Mater. **12**, 385 (2010).
[29] B. Yang, C. Motz, M. Rester, and G. Dehm, Yield stress influenced by the ratio of wire diameter to grain size—A competition between the effects of specimen microstructure and dimension in micro-sized polycrystalline copper wires, Philos. Mag. **92**, 3243 (2012).
[30] C. Shin, S. Lim, H.-h. Jin, P. Hosemann, and J. Kwon, Specimen size effects on the weakening of a bulk metastable austenitic alloy, Mater. Sci. Eng. A **622**, 67 (2015).
[31] N. Hansen, Hall-Petch relation and boundary strengthening, Scr. Mater. **51**, 801 (2004).
[32] M. A. Meyers and K. K. Chawla, *Mechanical Behavior of Materials*, 2nd ed. (Cambridge University Press, Cambridge, England, 2009).
[33] X. Xiao, Q. Chen, H. Yang, H. Duan, and J. Qu, A mechanistic model for depth-dependent hardness of ion irradiated metals, J. Nucl. Mater. **485**, 80 (2017).
[34] A. Ramar and R. Schäublin, Analysis of hardening limits of oxide dispersion strengthened steel, J. Nucl. Mater. **432**, 323 (2013).
[35] See Supplemental Material at http://link.aps.org/supplemental/10.1103/PhysRevLett.124.235501 for the yield strength predictions of other crystalline metallic materials, including Ni-based alloy, bi-crystal Cu and ultra-fine grain Cu.
[36] D. M. Dimiduk, M. D. Uchic, S. I. Rao, C. Woodward, and T. A. Parthasarathy, Overview of experiments on micro-crystal plasticity in FCC-derivative materials: Selected challenges for modelling and simulation of plasticity, Model. Simul. Mater. Sci. Eng. **15**, 135 (2007).
[37] M. D. Uchic and D. M. Dimiduk, A methodology to investigate size scale effects in crystalline plasticity using uniaxial compression testing, Mater. Sci. Eng. A **400–401**, 268 (2005).
[38] C. P. Frick, S. Orso, and E. Arzt, Loss of pseudoelasticity in nickel–titanium sub-micron compression pillars, Acta Mater. **55**, 3845 (2007).
[39] E. O. Hall, The deformation and ageing of mild steel: III Discussion of results, Proc. Phys. Soc. B **64**, 747 (1951).
[40] N. J. Petch, The cleavage strength of polycrystals, J. Iron Steel Inst. **174**, 25 (1953).
[41] J. C. M. Li, Petch relation and grain boundary sources, Trans. Metall. Soc. AIME **227**, 239 (1963).
[42] Y. Lin, J. Pan, Z. Luo, Y. Lu, K. Lu, and Y. Li, A grain-size-dependent structure evolution in gradient-structured (GS) Ni under tension, Nano Mater. Sci., **2**, 39 (2020).
[43] Z. Shan, E. A. Stach, J. M. K. Wiezorek, J. A. Knapp, D. M. Follstaedt, and S. X. Mao, Grain boundary-mediated plasticity in nanocrystalline nickel, Science **305**, 654 (2004).
[44] T. J. Rupert, D. S. Gianola, Y. Gan, and K. J. Hemker, Experimental observations of stress-driven grain boundary migration, Science **326**, 1686 (2009).
[45] J. Hu, Y. N. Shi, X. Sauvage, G. Sha, and K. Lu, Grain boundary stability governs hardening and softening in extremely fine nanograined metals, Science **355**, 1292 (2017).
[46] N. Hansen and B. Ralph, The strain and grain size dependence of the flow stress of copper, Acta Metall. **30**, 411 (1982).

[47] G. Khatibi, R. Stickler, V. Gröger, and B. Weiss, Tensile properties of thin Cu-wires with a bamboo microstructure, J. Alloys Compd. **378**, 326 (2004).

[48] D. Hull and D. J. Bacon, *Introduction to Dislocations*, 5th ed. (Butterworth-Heinemann, Oxford, 2011).

[49] N. V. Malyar, J. S. Micha, G. Dehm, and C. Kirchlechner, Size effect in bi-crystalline micropillars with a penetrable high angle grain boundary, Acta Mater. **129**, 312 (2017).

[50] N. V. Malyar, J. S. Micha, G. Dehm, and C. Kirchlechner, Dislocation-twin boundary interaction in small scale Cu bi-crystals loaded in different crystallographic directions, Acta Mater. **129**, 91 (2017).

[51] L. L. Li, X. H. An, P. J. Imrich, P. Zhang, Z. J. Zhang, G. Dehm, and Z. F. Zhang, Microcompression and cyclic deformation behaviors of coaxial copper bicrystals with a single twin boundary, Scr. Mater. **69**, 199 (2013).

[52] C. Howard, D. Frazer, A. Lupinacci, S. Parker, R. Z. Valiev, C. Shin, B. William Choi, and P. Hosemann, Investigation of specimen size effects by in-situ microcompression of equal channel angular pressed copper, Mater. Sci. Eng. A **649**, 104 (2016).

Supplementary Material for "Unified Model for Size-Dependent to Size-Independent Transition in Yield Strength of Crystalline Metallic Materials"

Wenbin Liu,[1] Ying Liu,[1] Yangyang Cheng,[1] Lirong Chen,[1] Long Yu,[1] Xin Yi,[1] and Huiling Duan[1,2]

[1]*State Key Laboratory for Turbulence and Complex Systems, Department of Mechanics and Engineering Science, BIC-ESAT, College of Engineering, Peking University, Beijing 100871, People's Republic of China*

[2]*CAPT, HEDPS and IFSA Collaborative Innovation Center of MoE, Peking University, Beijing 100871, People's Republic of China*

Part 1: Size effects of the yield strength for Ni-based alloy and pure Ni single crystals

In Fig. S1, we compare our theoretical predictions with the measured critical resolved shear stress (CRSS) of Ni-based alloy and pure Ni single crystals at different micropillar diameters. In experiments a significant size effect is observed in the pure Ni single crystal, whereas the CRSS of Ni-based alloy is size-independent. In the model predictions by Eq. (3) with $\tau_m = \tau_f + \alpha\mu b\sqrt{\rho_{\text{dis}}} + \Delta\tau$, we have used the dispersed barrier hardening model $\Delta\tau = \beta\mu b\sqrt{N_{\text{def}} d_{\text{def}}}$ to characterize the oxide dispersion induced hardening in Ni-based alloy [1], where β is the hardening coefficient, N_{def} and d_{def} are the average density and size of the oxide particles [2], respectively. The model parameters are listed in Table S1. According to theoretical results, it is known that, at $d > 200$ nm, the yield strength of Ni-based alloy single crystals is controlled by the dislocation motion stress, which is size-independent. Meanwhile, the size dependence of yield strength for pure Ni single crystals is determined by the source activation stress. As d exceeds 2 μm, the behavior of transition from size-dependent to size-independent can be observed for the yield strength of pure Ni single crystals, consistent with experimental results. Here the dislocation density of microcrystals is estimated as $\rho_{\text{dis}} = 7\times10^{12}$ m^{-2}, which is very closed to $\rho_{\text{dis}} = 5\times10^{12}$ m^{-2} estimated by Dimiduk et al. [3]

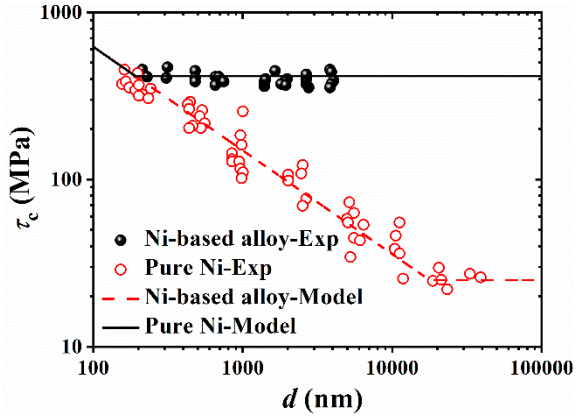

FIG. S1. CRSS τ_c as a function of the pillar diameter d for Ni-based alloy and pure Ni single crystals. Symbols represent experimental data from Refs. [2] (alloy), [3] and [4] (pure Ni).

Table S1. Parameters for model prediction of Ni-based alloy and pure Ni single crystals.

Materials	μ (GPa)	b (nm)	K (m^{m-1})	m	α	β (N/m)	N_{def} (m^{-3})	d_{def} (nm)	ρ_{dis} (m^{-2})
Ni alloy	76[a]	0.249[a]	1500	0.62	0.5[a]	0.62	1.1×10^{23} [b]	30[b]	7×10^{12}
Pure Ni	76[a]	0.249[a]	1500	0.62	0.5[a]	-	-	-	7×10^{12}

Parameters with superscripts *a* and *b* are adopted from Refs. [5] and [2], respectively.

Part 2: Yield stresses for Cu and austenitic stainless steel polycrystalline materials

The size dependence of normalized yield stress $\sigma_y / \sigma_y^{bulk}$ for Cu and austenitic stainless steel is presented in Fig. S2. Symbols represent the experimental data, and lines represent the model predictions given by Eq. (10) with various single crystal yield stress τ_0 and grain size d.

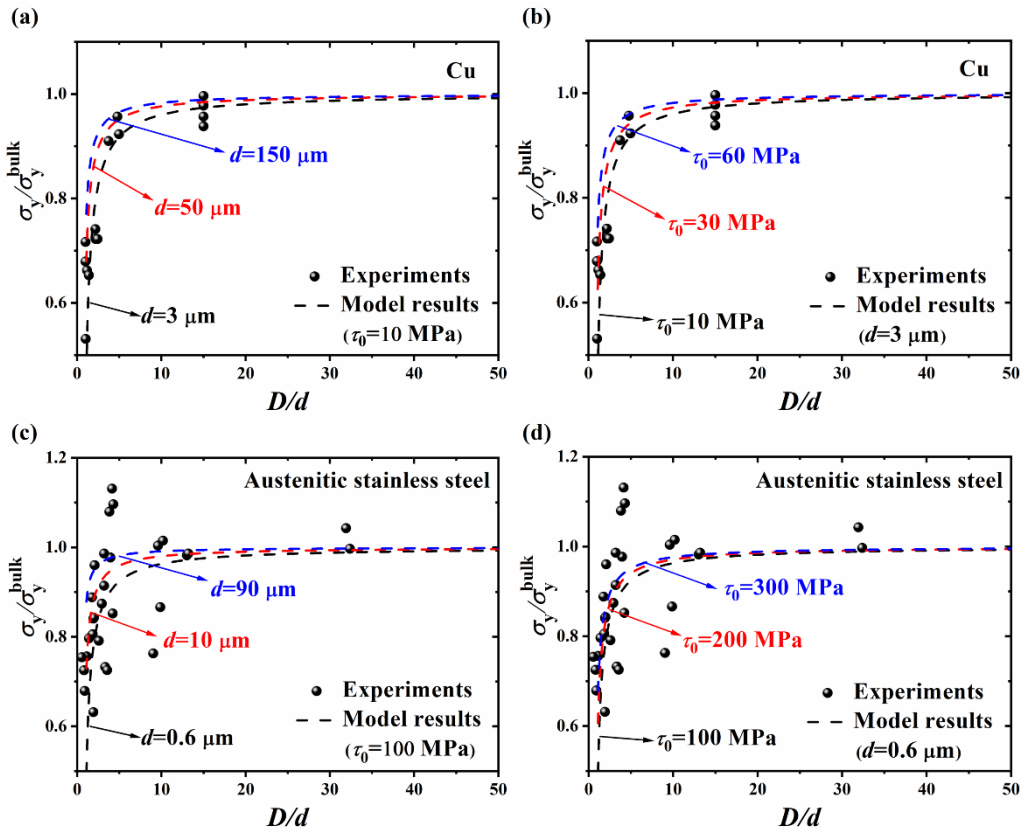

FIG. S2. Size dependence of normalized yield stress $\sigma_y / \sigma_y^{bulk}$ for (a-b) Cu [6] and (c-d) austenitic stainless steel [7] polycrystal samples. (a,c) Model predictions for different values of d. (b,d) Model predictions for various τ_0. The material constant k is taken as $0.06\ \text{MPa}\cdot\sqrt{\text{m}}$ and $0.2\ \text{MPa}\cdot\sqrt{\text{m}}$ for Cu and austenitic stainless steels, respectively.

Part 3: Yield stress for bi-crystal Cu

The present model suggests that the polycrystalline samples with the small enough grain size have the same yield strength as the single crystal components. The micro-compression tests on bi-crystal Cu with high angle GB [8] are used to verify this model.

Figure S3(a) displays σ_y as a function of the grain size d for Cu bi-crystals and the corresponding single crystals. A good agreement is observed between the experimental results and Eq. (11) with model parameters listed in Table S2. The contribution of GB hardening effect is $0.02\sqrt{2/(\pi d)}$ MPa for the cylindrical bi-crystals with $S_V = 2/(\pi d)$ taking $k = 0.06\ \text{MPa}\cdot\sqrt{\text{m}}$ ($k^* \approx 0.02\ \text{MPa}\cdot\sqrt{\text{m}}$). The yield stresses of both single crystals exhibit the size effect, indicating that the source activation dominates the material yielding. The mean yield stress of grains A and B is presented in the bi-crystal, i.e. $\sigma_y = (\tau_c^{\text{A}} / R^{\text{A}} + \tau_c^{\text{B}} / R^{\text{B}})/2$. It means that the high angle GB does not strengthen the yield stress as $\tau_m > \tau_s$. Such an identical phenomena has been observed in the Cu bi-crystal with a twin boundary [9, 10] and ultrafine grain Cu [11] (as detailed in Fig. S4).

Figure S3(b) shows the competition between the stress required for source activation and dislocation motion in the Cu bi-crystal. With the increases of d, the decrease of GB density leads to a decrease of the dislocation motion stress, and the source activation stress also decreases. As d exceeds 200 μm, the yield strength of the bi-crystal shows a transition from dislocation source-controlled to dislocation motion-controlled.

Table S2. Parameters for model prediction of single components in bi-crystal Cu.

Materials	μ (GPa)	b (nm)	K (m^{m-1})	m	α	R	ρ_{dis} (m^{-2})
Grain A	48.3[a]	0.255[a]	3.5×10^2	0.7	0.5[a]	0.43[b]	2×10^{12}
Grain B	48.3[a]	0.255[a]	9.5×10^3	0.45	0.5[a]	0.44[b]	2×10^{12}

Parameters with superscripts *a* and *b* are adopted from Refs. [5] and [8], respectively.

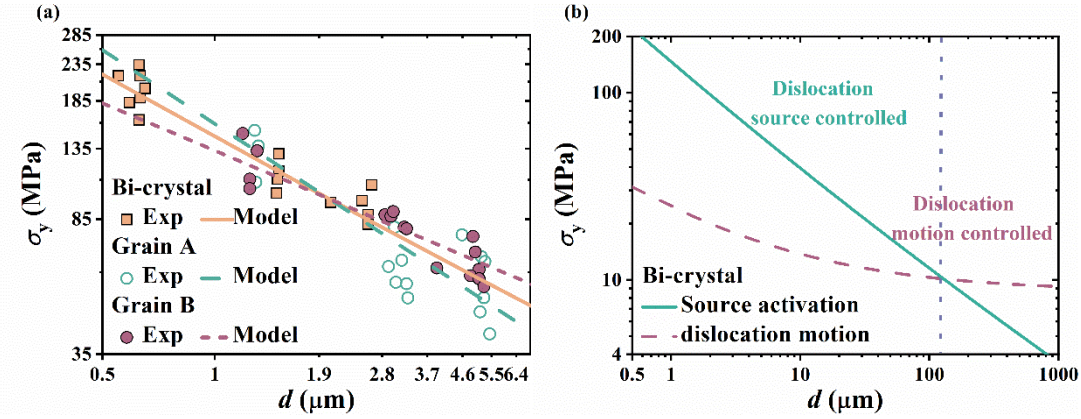

FIG. S3. Size-dependent yield stress σ_y for Cu bi-crystal (a) and a contribution from two components: source activation and dislocation motion (b). Symbols in (a) denote experimental data from Ref. [8].

Part 4: Yield stress for ultrafine grain Cu crystals

Figure S4 displays σ_y as a function of D/d for ultrafine grain Cu with a grain size of $d \approx 200$ nm. The stress required for dislocation motion and dislocation source activation is calculated by Eq. (11) and Taylor factor $M \approx 3$. The model parameters are listed as Table S3.

In Fig. S4, there are no size effects of yield strength shown in the experimental results of

ultrafine grain Cu. The micropillars containing several grains exhibit the same yield strength with bulk pillars, although the dislocation motion stress increases with D/d due to the increasing density of grain boundaries. It means that the yield stress of ultrafine grain Cu is not controlled by the dislocation motion stress. As shown in Fig. S4, the stress required for dislocation motion is larger than that for source activation in a wide range of D/d, and the model prediction agrees well with the experimental results. Therefore, one can conclude that the source activation stress dominates the yield stress of the ultrafine grain Cu over a wide range of sample sizes.

Table S3. Parameters for model prediction of ultrafine grain Cu.

Material	μ (GPa)	b (nm)	K (m^{m-1})	m	α	k (MPa$\sqrt{m}$)	ρ_{dis} (m^{-2})
Ultrafine grain Cu	48.3[a]	0.255[a]	1×10^3	0.6	0.5[a]	0.02	8×10^{13}

Parameters with superscript *a* are adopted from Ref. [5].

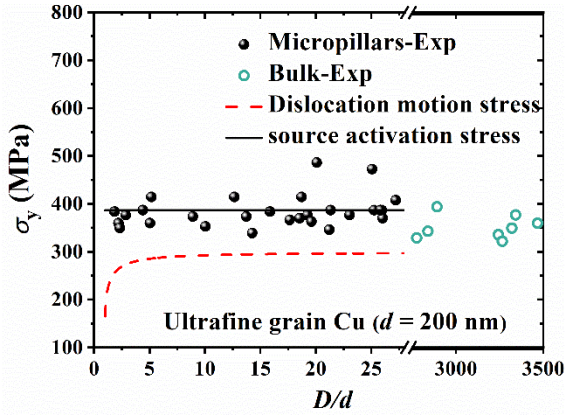

FIG. S4. σ_y as a function of D/d for ultrafine grain Cu with grain size d =200 nm. Symbols are experimental results from Ref. [11].

References

[1] A. Ramar and R. Schäublin, Analysis of hardening limits of oxide dispersion strengthened steel, J. Nucl. Mater. **432**, 323 (2013).

[2] B. Girault, A. S. Schneider, C. P. Frick, and E. Arzt, Strength effects in micropillars of a dispersion strengthened superalloy, Adv. Eng. Mater. **12**, 243 (2010).

[3] D. M. Dimiduk, M. D. Uchic, and T. A. Parthasarathy, Size-affected single-slip behavior of pure nickel microcrystals, Acta Mater. **53**, 4065 (2005).

[4] C. P. Frick, B. G. Clark, S. Orso, A. S. Schneider, and E. Arzt, Size effect on strength and strain hardening of small-scale [111] nickel compression pillars, Mater. Sci. Eng. A **489**, 319 (2008).

[5] M. A. Meyers and K. K. Chawla, *Mechanical Behavior of Materials*, 2nd ed. (Cambridge University Press, Cambridge, UK, 2009).

[6] B. Yang, C. Motz, M. Rester, and G. Dehm, Yield stress influenced by the ratio of wire diameter to grain size – A competition between the effects of specimen microstructure and

dimension in micro-sized polycrystalline copper wires, Philos. Mag. **92**, 3243 (2012).
[7] C. Shin, S. Lim, H.-h. Jin, P. Hosemann, and J. Kwon, Specimen size effects on the weakening of a bulk metastable austenitic alloy, Mater. Sci. Eng. A **622**, 67 (2015).
[8] N. V. Malyar, J. S. Micha, G. Dehm, and C. Kirchlechner, Size effect in bi-crystalline micropillars with a penetrable high angle grain boundary, Acta Mater. **129**, 312 (2017).
[9] N. V. Malyar, J. S. Micha, G. Dehm, and C. Kirchlechner, Dislocation-twin boundary interaction in small scale Cu bi-crystals loaded in different crystallographic directions, Acta Mater. **129**, 91 (2017).
[10] L. L. Li, X. H. An, P. J. Imrich, P. Zhang, Z. J. Zhang, G. Dehm, and Z. F. Zhang, Microcompression and cyclic deformation behaviors of coaxial copper bicrystals with a single twin boundary, Scr. Mater. **69**, 199 (2013).
[11] C. Howard, D. Frazer, A. Lupinacci, S. Parker, R. Z. Valiev, C. Shin, B. William Choi, and P. Hosemann, Investigation of specimen size effects by in-situ microcompression of equal channel angular pressed copper, Mater. Sci. Eng. A **649**, 104 (2016).